Enzyme Models

DOI: 10.1002/anie.200802672

Reactive Intermediates in Oxygenation Reactions with Mononuclear Nonheme Iron Catalysts**

*Jihae Yoon, Samuel A. Wilson, Yu Kyeong Jang, Mi Sook Seo, Kasi Nehru, Britt Hedman, Keith O. Hodgson, Eckhard Bill, Edward I. Solomon, and Wonwoo Nam**

Mononuclear nonheme iron oxygenases catalyze a diverse array of important metabolic transformations that require the binding and activation of dioxygen.[1] In the catalytic cycles of the nonheme iron enzymes, several intermediates, such as iron(III) hydroperoxo, iron(IV) oxo, and iron(V) oxo species, have been proposed as active oxidants that effect the oxygenation of organic substrates.[2] Among the proposed intermediates, synthetic nonheme iron(III) hydroperoxo species were shown to be sluggish oxidants that cannot oxygenate organic substrates such as alkanes and olefins.[3]

The first nonheme iron(IV) oxo complex was characterized spectroscopically by Wieghardt and co-workers.[4] Subsequently, a crystal structure of a nonheme iron(IV) oxo complex was reported by Rohde et al.[5] Since then, a handful of iron(IV) oxo complexes have been synthesized and investigated in various oxidation reactions,[6,7] which have demonstrated that nonheme iron(IV) oxo species are capable of oxygenating organic substrates, such as alkanes, alkenes, alcohols, and sulfides.

Iron(V) oxo species have also been inferred as active oxidants in the oxygenation of organic substrates by nonheme iron catalysts.[8] Although such an iron(V) oxo intermediate was synthesized and characterized by various spectroscopic techniques,[9] evidence for the involvement of iron(V) oxo species as active oxidants in catalytic oxygenation reactions was indirect and mainly came from product analysis, such as a selectivity of alcohol over ketone groups in alkane hydroxylation, a kinetic isotope effect (KIE) value greater than 4, and the incorporation of ^{18}O from $H_2{}^{18}O$ into the products of isotopic labeling experiments.[8] However, iron(IV) oxo complexes have also shown very large KIE values[7] and oxygen exchange with $H_2{}^{18}O$.[10] Therefore, it is difficult to distinguish the nature of the intermediate(s) (e.g., iron(IV) oxo vs. iron(V) oxo species) in catalytic oxygenation reactions.

Herein, we report a new nonheme iron(IV) oxo complex, $[Fe^{IV}(O)(bqen)]^{2+}$ (**1**; bqen=*N*,*N*′-dimethyl-*N*,*N*′-bis(8-quinolyl)ethane-1,2-diamine, Figure 1), which shows a high reactivity in the oxidation reactions of alkanes and alcohols. Reactivity studies revealed that the alkane and alcohol oxidations occur by a hydrogen-atom abstraction mechanism. We have also obtained strong evidence that an intermediate that is different from the iron(IV) oxo species is involved in the catalytic oxidation of alkanes and alcohols by an iron catalyst and a terminal oxidant.

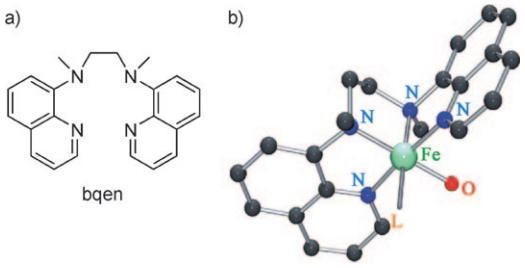

Figure 1. Schematic representation of a) the bqen ligand and b) $[Fe^{IV}(O)(bqen)(CH_3CN)]^{2+}$ (**1**, L = CH_3CN).

The reaction of $[Fe^{II}(bqen)](CF_3SO_3)_2$[11] with CH_3CO_3H in CH_3CN at 0 °C produced a green intermediate **1** with λ_{max} at 740 nm (Figure 2a). This chromophore resembles those associated with $S = 1$ nonheme iron(IV) oxo complexes.[4–7,12] The EPR spectrum of **1** appeared silent, as observed in other iron(IV) oxo species.[5–7] The ESI mass spectrum of **1** shows a prominent ion peak at *m*/*z* 563.0 (Figure 2b), which shifts to *m*/*z* 565.0 upon introduction of $H_2{}^{18}O$ into the solution of **1** (see Figure S1 in the Supporting Information for mass spectral changes of **1** at different incubation times), which indicates that **1** contains an iron oxo group that exchanges its oxygen atom with $H_2{}^{18}O$ at a slow rate.[10] These mass spectral data are consistent with the formulation of **1** as $[Fe^{IV}(O)(bqen)(CF_3SO_3)]^+$ (calculated *m*/*z* 563.1).

The formation of an iron(IV) oxo species in the reaction of $[Fe^{II}(bqen)]^{2+}$ and CH_3CO_3H was further confirmed by X-ray absorption spectroscopy (XAS; Figure 3a). The Fe K XAS pre-edge and edge of intermediate **1** show an

[*] J. Yoon, Y. K. Jang, Dr. M. S. Seo, K. Nehru, Prof. Dr. W. Nam
Department of Chemistry and Nano Science, Department of Bioinspired Science, Ewha Womans University
Seoul 120–750 (Korea)
Fax: (+82) 2-3277-4441
E-mail: wwnam@ewha.ac.kr
S. A. Wilson, B. Hedman, Prof. Dr. K. O. Hodgson, Prof. Dr. E. I. Solomon
Department of Chemistry, Stanford University (USA)
Dr. E. Bill
Max-Planck-Institut für Bioanorganische Chemie
Mülheim (Germany)

[**] The research at EWU was supported by KOSEF/MOST through the CRI Program and the WCU project, Korea, and that at Stanford University by NIH grants RR-01209 (K.O.H.) and GM 40392 (E.I.S.). SSRL operations is funded by the US DOE BES, and the SSRL SMB program by NIH NCRR BTP and DOE BER. The project described was supported by grant no. 5 P41 RR001209 from the National Center for Research Resources (NCRR), a component of the National Institutes of Health (NIH), and its contents are solely the responsibility of the authors and do not necessarily represent the official view of the NCRR or the NIH.

Supporting information for this article is available on the WWW under http://dx.doi.org/10.1002/anie.200802672.

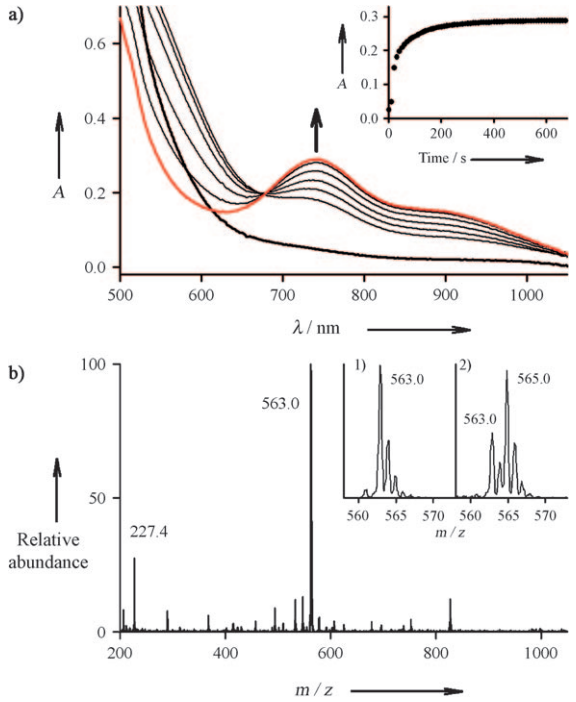

Figure 2. a) UV/Vis spectral changes showing the formation of **1** (red bold line) in the reaction of $[Fe^{II}(bqen)](CF_3SO_3)_2$ (2 mM, black bold line) and CH_3CO_3H (6 mM) in CH_3CN at 0 °C. b) ESI-MS spectrum of **1**. The ion peak at *m*/*z* 227.4 corresponds to $[Fe^{IV}(O)(bqen)(CH_3CN)]^{2+}$. The inset shows observed isotope distribution patterns for 1) $[^{16}O]$-**1** and 2) a mixture of $[^{16}O]$-**1** (37%) and $[^{18}O]$-**1** (63%). The latter ESI-MS spectrum was obtained by generating **1** in the reaction of $[Fe^{II}(bqen)](CF_3SO_3)_2$ (2 mM) and CH_3CO_3H (6 mM) in the presence of $H_2{}^{18}O$ (20 μL) in CH_3CN at 0 °C.

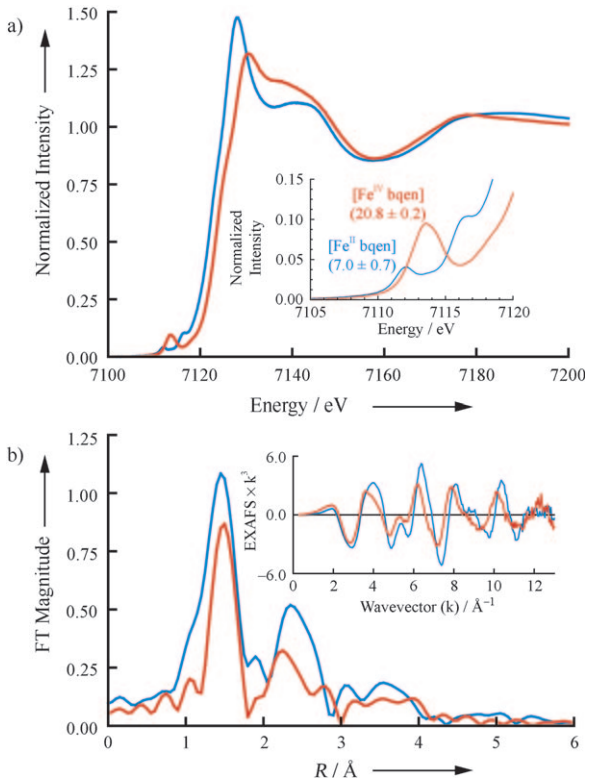

Figure 3. a) Fe X-ray absorption spectra showing the normalized edge and XANES regions. The inset shows the normalized pre-edge region. b) Overlay of the Fourier transform ($k = 2$–13 Å^{-1}) and EXAFS data (inset). Curves for $[Fe^{II}(bqen)]^{2+}$ are shown in blue and $[Fe^{IV}(O)(bqen)]^{2+}$ (**1**) in red.

increase in energy of about 2 eV relative to the starting material, as well as a notable increase in pre-edge intensity, from about 7 to about 21 units. The edge shift and increase in pre-edge intensity are a result of a greater Z_{eff} value and distortion from centrosymmetry, which indicates the presence of a short Fe^{IV}=O bond.[12c,13] The extended X-ray absorption fine structure (EXAFS) data for $[Fe^{II}(bqen)]^{2+}$ and **1** show a notable intensity decrease upon oxidation as well as a sharpening of the first shell feature in the Fourier transform (Figure 3b; see the Supporting Information for a detailed discussion, Table S2 gives the best EXAFS fits to $[Fe^{II}(bqen)]^{2+}$ (fit 3) and **1** (fit 4)). The EXAFS data for $[Fe^{II}(bqen)]^{2+}$ fit to a six-coordinate first shell of light atoms (nitrogen or carbon) at 1.97 Å, whereas a short 1.67 Å Fe^{IV}=O bond is required to accurately fit the EXAFS data for **1**. The decrease in EXAFS amplitude and Fourier transform intensity could be a result of the combination of the formation of a short Fe^{IV}=O bond and the presence of a mixture because of the incomplete conversion to **1**. The short Fe=O bond causes a lengthening of the *trans* Fe–N bond (see the Supporting Information for XAS results and DFT analysis), which results in a less-ordered first shell. Sharpening of the Fourier transform over the first shell might be a result of the EXAFS wave contribution from the short Fe^{IV}=O bond, as the short EXAFS wave overlaps with the main first-shell feature, which creates destructive interference at high and low *k* value or from interference from the signals of the starting material (a more detailed analysis of both the pre-edge and EXAFS fits is given in the Supporting Information).

The intermediate **1** has a significant lifetime ($t_{1/2} \approx 30$ minutes) at 0 °C, which decayed at a fast rate upon addition of substrates, such as triphenylmethane, indan, tetralin, cumene, ethylbenzene, and benzyl alcohol. Pseudo-first-order fitting of the kinetic data allowed us to determine k_{obs} values, and the pseudo-first-order rate constants increased linearly with the increase of substrate concentration (Figure S4 in the Supporting Information); the second-order rate constants, k_2, at 0 °C were 2.4×10^{-1} M^{-1} s^{-1} for triphenylmethane, 4.5×10^{-1} M^{-1} s^{-1} for indan, 4.3×10^{-1} M^{-1} s^{-1} for tetralin, 2.7×10^{-2} M^{-1} s^{-1} for cumene, 2.6×10^{-2} M^{-1} s^{-1} for ethylbenzene, and 6.7×10^{-1} M^{-1} s^{-1} for benzyl alcohol. When the log k_2' values (k_2 adjusted for reaction stoichiometry) were plotted against the C–H bond dissociation energy (BDE) of the substrates (triphenylmethane, 81 kcal mol^{-1}; indan, 82 kcal mol^{-1}; tetralin, 82 kcal mol^{-1}; cumene, 85 kcal mol^{-1}; ethylbenzene, 87 kcal mol^{-1}),[14] we have obtained a linear correlation between the reaction rates and the C–H BDE of substrates (Figure 4). The observation that the rate constants decrease with the increase of the C–H BDE of the substrates implicates an H-atom abstraction as the rate-determining step for the oxidation.[15] Further evidence for the H-atom abstraction mechanism was obtained from the measurement of KIE values in the oxidation of cumene, ethylbenzene, and

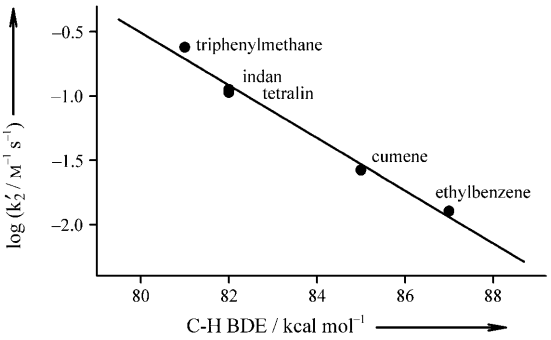

Figure 4. Plot of log k_2' of **1** against the C–H BDE of substrates. Second-order rate constants, k_2, were determined at 0 °C and then adjusted for reaction stoichiometry to give k_2' based on the number of equivalent target C–H bonds of substrates (that is, one for triphenylmethane and cumene, two for ethylbenzene, and four for indan and tetralin).

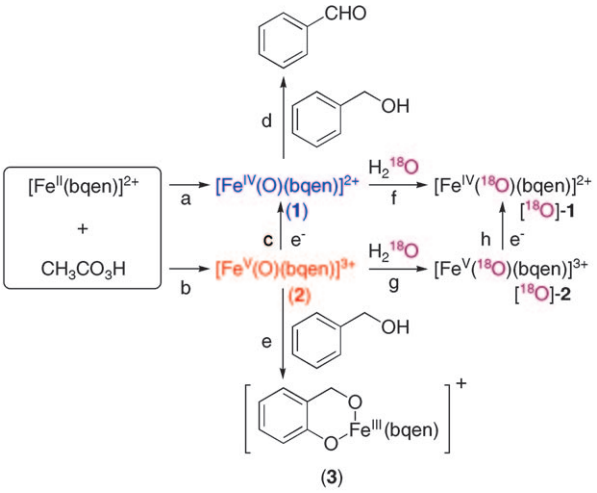

Scheme 1. Reactions of an in situ generated iron(IV) oxo species (**1**) and a proposed iron(V) oxo species (**2**) under stoichiometric and catalytic conditions, respectively.

benzyl alcohol; KIE values of 25(2) for benzyl alcohol, and values greater than 11 for cumene, and 10 for ethylbenzene are consistent C–H bond cleavage being the rate-determining step (Table S3 in the Supporting Information).[16] It noteworthy that large KIE values of 30–50 were reported in the oxidation of ethylbenzene and benzyl alcohol by $[Fe^{IV}(O)(N4Py)]^{2+}$ (N4Py = *N*,*N*-bis(2-pyridylmethyl)-*N*-bis(2-pyridyl)methylamine)[7a,b] and in the cleavage of the target C–H bond of taurine by the Fe^{IV}=O intermediate of taurine:α-ketoglutarate dioxygenase (TauD).[17] The good correlation between reaction rates and BDE of substrates and large KIE values in the C–H bond oxidation of alkanes and alcohol support the notion that the oxidation of alkanes and alcohols by **1** occurs by an H-atom abstraction mechanism.[7,17]

Interestingly, when CH_3CO_3H was added to a solution containing $[Fe^{II}(bqen)]^{2+}$ and indan at 0 °C, the formation of **1** was not observed (Figure S5a in the Supporting Information). Considering the reaction rate of **1** with indan at 0 °C (Figure S5b in the Supporting Information), this result implies that a highly reactive intermediate **2** was generated in the reaction of $[Fe^{II}(bqen)]^{2+}$and CH_3CO_3H and then reacted fast with indan. If **1** is the sole intermediate generated in the reaction of $[Fe(bqen)]^{2+}$ and CH_3CO_3H, the formation of **1** should be observed even in the presence of indan and then the decay of **1** by reaction with the substrate (Figure S5b in the Supporting Information).

The following observations further support the involvement of **2** as an active species in the reaction of $[Fe^{II}(bqen)]^{2+}$and CH_3CO_3H under catalytic conditions. When the oxidation of benzyl alcohol by $[Fe^{II}(bqen)]^{2+}$and CH_3CO_3H was carried out at 0 °C, a deep green color developed within 60 seconds (λ_{max} = 660 nm; Figure S6a in the Supporting Information). The ESI mass spectrum of the green species **3** shows a prominent peak at *m*/*z* 520.1 (calculated *m*/*z* 520.2; Figure S6b in the Supporting Information), the mass and isotope distribution pattern of which corresponds to $[Fe^{III}(bqen)\{OCH_2(C_6H_4)O\}]^+$ (see the proposed structure **3** in Scheme 1). The EPR spectrum of **3** shows a strong signal at g = 4.3, which is typical of a high-spin (S = 5/2) Fe^{III} species (Figure S6c in the Supporting Information). The spectroscopic observations indicate that the aromatic ring hydroxylation of benzyl alcohol took place at the *ortho* position, which affords an iron(III) complex that bears a 2-hydroxybenzyl alcohol ligand (Scheme 1, pathway e).[18] This proposal is based on recent reports that reactions of nonheme iron(II) complexes that bear two *cis*-labile sites, such as $[Fe(tpa)]^{2+}$ (tpa = tris(2-pyridylmethyl)amine) and $[Fe(bpmen)]^{2+}$ (bpmen = *N*,*N*′-dimethyl-*N*,*N*′-bis(2-pyridylmethyl)ethane-1,2-diamine), react with perbenzoic acids or benzoic acid and H_2O_2 to afford iron(III) salicylate complexes.[19] We therefore propose that the aromatic ring hydroxylation is a preferred pathway in the oxidation of benzyl alcohol by the intermediate **2**. In contrast, the formation of **3** was not observed in the reaction of **1** and benzyl alcohol, which demonstrates that **1** does not hydroxylate the aromatic ring of benzyl alcohol but oxidizes benzyl alcohol to benzaldehyde (Scheme 1, pathway d).

By carrying out isotopic labeling experiments, the intermediate **2** was found to contain an iron oxo group that was exchangeable with $H_2{}^{18}O$ at a fast rate. We have shown above that the iron oxo group of **1** exchanges with $H_2{}^{18}O$ at a slow rate (that is, ca. 50 % ^{18}O exchange after 20 minutes incubation; Scheme 1, pathway f and Figure S1 in the Supporting Information). Interestingly, when **1** was generated in the presence of $H_2{}^{18}O$ in the reaction of $[Fe^{II}(bqen)]^{2+}$ and CH_3CO_3H and analyzed immediately (that is, less than 30 seconds) by ESI-MS, we found that **1** contained about 63 % ^{18}O derived from $H_2{}^{18}O$ (see the inset in Figure 2b). These results imply that **2** exchanges its oxygen atom with $H_2{}^{18}O$ at a fast rate (Scheme 1, pathway g), followed by the conversion of **2** to **1** (Scheme 1, pathway h). The present results further indicate that the proposed iron(V) oxo species exchanges its oxygen with $H_2{}^{18}O$ much faster than the corresponding iron(IV) oxo species. This speculation is of interest since the dependence of the oxygen exchange of metal oxo species on the oxidation states of metal ions has never been explored previously,[20] and we are currently investigating the effect of the metal oxidation states on the oxygen exchange between high-valent metal oxo complexes

and $H_2{}^{18}O$ under identical conditions (that is, the same ligand structure and solvent systems).

Finally, we propose the mechanism for the formation of **1** and **2** in the reaction of $[Fe^{II}(bqen)]^{2+}$ and CH_3CO_3H as follows: $[Fe^{II}(bqen)]^{2+}$ is oxidized to $[Fe^{III}(bqen)]^{3+}$ by CH_3CO_3H.[21] Then, $[Fe^{III}(bqen)\{OO(C{=}O)CH_3\}]^{2+}$ is generated by the reaction of $[Fe^{III}(bqen)]^{3+}$ and CH_3CO_3H. The O–O bond heterolysis of $[Fe^{III}(bqen)\{OO(C{=}O)CH_3\}]^{2+}$ produces **2**, followed by one-electron reduction of the unstable **2** that leads to the formation of **1**.[22] Nonetheless, other high-valent iron oxo species, such as $[Fe^{IV}(OH)_2(bqen)]^{2+}$ and the high-spin ($S=2$) $[Fe^{IV}(O)(bqen)]^{2+}$,[23] can be considered as plausible structures for **2**.

In conclusion, we have reported the synthesis, characterization, and reactivities of a mononuclear nonheme iron(IV) oxo complex, $[Fe^{IV}(O)(bqen)]^{2+}$ (**1**). We have also provided strong evidence that an intermediate different from **1**, possibly an iron(V) oxo species (**2**), is involved as an active oxidant in the catalytic oxidation of alkanes and alcohols by $[Fe^{II}(bqen)]^{2+}$ and peracetic acid. The reactivity of **2** is greater than that of **1**, the product distributions observed in the reactions of **1** and **2** are different, and **2** exchanges its oxygen with $H_2{}^{18}O$ much faster than **1**. Future studies will focus on attempts to characterize the intermediate **2** and understand the reactivity of **2** in various oxygenation reactions.

Received: June 6, 2008
Revised: November 19, 2008
Published online: January 9, 2009

Keywords: bioinorganic chemistry · C–H activation · enzyme models · iron · oxidation

[1] a) C. Krebs, D. G. Fujimori, C. T. Walsh, J. M. Bollinger, Jr., *Acc. Chem. Res.* **2007**, *40*, 484–492; b) M. M. Abu-Omar, A. Loaiza, N. Hontzeas, *Chem. Rev.* **2005**, *105*, 2227–2252; c) M. Costas, M. P. Mehn, M. P. Jensen, L. Que, Jr., *Chem. Rev.* **2004**, *104*, 939–986.

[2] L. Que, Jr., *J. Biol. Inorg. Chem.* **2004**, *9*, 684–690.

[3] a) M. J. Park, J. Lee, Y. Suh, J. Kim, W. Nam, *J. Am. Chem. Soc.* **2006**, *128*, 2630–2634; b) M. S. Seo, T. Kamachi, T. Kouno, K. Murata, M. J. Park, K. Yoshizawa, W. Nam, *Angew. Chem.* **2007**, *119*, 2341–2344; *Angew. Chem. Int. Ed.* **2007**, *46*, 2291–2294.

[4] C. A. Grapperhaus, B. Mienert, E. Bill, T. Weyhermüller, K. Wieghardt, *Inorg. Chem.* **2000**, *39*, 5306–5317.

[5] J.-U. Rohde, J.-H. In, M. H. Lim, W. W. Brennessel, M. R. Bukowski, A. Stubna, E. Münck, W. Nam, L. Que, Jr., *Science* **2003**, *299*, 1037–1039.

[6] a) W. Nam, *Acc. Chem. Res.* **2007**, *40*, 522–531; b) L. Que, Jr., *Acc. Chem. Res.* **2007**, *40*, 493–500.

[7] a) J. Kaizer, E. J. Klinker, N. Y. Oh, J.-U. Rohde, W. J. Song, A. Stubna, J. Kim, E. Münck, W. Nam, L. Que, Jr., *J. Am. Chem. Soc.* **2004**, *126*, 472–473; b) N. Y. Oh, Y. Suh, M. J. Park, M. S. Seo, J. Kim, W. Nam, *Angew. Chem.* **2005**, *117*, 4307–4311; *Angew. Chem. Int. Ed.* **2005**, *44*, 4235–4239; c) C. V. Sastri, J. Lee, K. Oh, Y. J. Lee, J. Lee, T. A. Jackson, K. Ray, H. Hirao, W. Shin, J. A. Halfen, J. Kim, L. Que, Jr., S. Shaik, W. Nam, *Proc. Natl. Acad. Sci. USA* **2007**, *104*, 19181–19186.

[8] a) K. Chen, L. Que, Jr., *Chem. Commun.* **1999**, 1375–1376; b) M. Costas, K. Chen, L. Que, Jr., *Coord. Chem. Rev.* **2000**, *200–202*, 517–544; c) R. Mas-Ballesté, L. Que, Jr., *J. Am. Chem. Soc.* **2007**, *129*, 15964–15972; d) S. H. Lee, J. H. Han, H. Kwak, S. J. Lee, E. Y. Lee, H. J. Kim, J. H. Lee, C. Bae, S. N. Lee, Y. Kim, C. Kim, *Chem. Eur. J.* **2007**, *13*, 9393–9398.

[9] F. T. de Oliveira, A. Chanda, D. Banerjee, X. Shan, S. Mondal, L. Que, Jr., E. L. Bominaar, E. Münck, T. J. Collins, *Science* **2007**, *315*, 835–838.

[10] M. S. Seo, J.-H. In, S. O. Kim, N. Y. Oh, J. Hong, J. Kim, L. Que, Jr., W. Nam, *Angew. Chem.* **2004**, *116*, 2471–2474; *Angew. Chem. Int. Ed.* **2004**, *43*, 2417–2420.

[11] J. England, G. J. P. Britovsek, N. Rabadia, A. J. P. White, *Inorg. Chem.* **2007**, *46*, 3752–3767.

[12] a) J. Bautz, M. R. Bukowski, M. Kerscher, A. Stubna, P. Comba, A. Lienke, E. Münck, L. Que, Jr., *Angew. Chem.* **2006**, *118*, 5810–5813; *Angew. Chem. Int. Ed.* **2006**, *45*, 5681–5684; b) A. Decker, J.-U. Rohde, L. Que, Jr., E. I. Solomon, *J. Am. Chem. Soc.* **2004**, *126*, 5378–5379; c) M. H. Lim, J.-U. Rohde, A. Stubna, M. R. Bukowski, M. Costas, R. Y. N. Ho, E. Münck, W. Nam, L. Que, Jr., *Proc. Natl. Acad. Sci. USA* **2003**, *100*, 3665–3670.

[13] T. E. Westre, P. Kennepohl, J. G. DeWitt, B. Hedman, K. O. Hodgson, E. I. Solomon, *J. Am. Chem. Soc.* **1997**, *119*, 6297–6314.

[14] a) J. R. Bryant, J. M. Mayer, *J. Am. Chem. Soc.* **2003**, *125*, 10351–10361; b) W. W. Y. Lam, S.-M. Yiu, D. T. Y. Yiu, T.-C. Lau, W.-P. Yip, C.-M. Che, *Inorg. Chem.* **2003**, *42*, 8011–8018.

[15] a) J. M. Mayer, *Acc. Chem. Res.* **1998**, *31*, 441–450; b) A. S. Borovik, *Acc. Chem. Res.* **2005**, *38*, 54–61.

[16] Since the reaction rates of **1** with deuterated cumene and ethylbenzene were the same as the natural decay of **1**, we were not able to determine the exact KIE values (see Table S3 in the Supporting Information).

[17] J. C. Price, E. W. Barr, T. E. Glass, C. Krebs, J. M. Bollinger, Jr., *J. Am. Chem. Soc.* **2003**, *125*, 13008–13009.

[18] The structure of the 2-hydroxybenzyl alcohol product was confirmed by comparing the ^{1}H NMR spectrum of the extract that was prepared by treating **2** with acid with the ^{1}H NMR spectrum of authentic 2-hydroxybenzyl alcohol (Figure S7 in the Supporting Information).

[19] a) N. Y. Oh, M. S. Seo, M. H. Lim, M. B. Consugar, M. J. Park, J.-U. Rohde, J. Han, K. M. Kim, J. Kim, L. Que, Jr., W. Nam, *Chem. Commun.* **2005**, 5644–5646; b) S. Taktak, M. Flook, B. M. Foxman, L. Que, Jr., E. V. Rybak-Akimova, *Chem. Commun.* **2005**, 5301–5303.

[20] a) W. J. Song, M. S. Seo, S. D. George, T. Ohta, R. Song, M.-J. Kang, T. Tosha, T. Kitagawa, E. I. Solomon, W. Nam, *J. Am. Chem. Soc.* **2007**, *129*, 1268–1277; b) J. T. Groves, J. Lee, S. S. Marla, *J. Am. Chem. Soc.* **1997**, *119*, 6269–6273; c) J. Bernadou, A.-S. Fabiano, A. Robert, B. Meunier, *J. Am. Chem. Soc.* **1994**, *116*, 9375–9376.

[21] The oxidation of nonheme iron(II) to iron(III) species has been well documented: See references [8a,b] and [19b].

[22] It is well known in iron porphyrin systems that $[Fe^{IV}(O)(porphyrin)]^{+\cdot}$ species are reduced to $[Fe^{IV}(O)(porphyrin)]$ in such reactions.

[23] a) J. Bautz, P. Comba, C. L. de Laorden, M. Menzel, G. Rajaraman, *Angew. Chem.* **2007**, *119*, 8213–8216; *Angew. Chem. Int. Ed.* **2007**, *46*, 8067–8070; b) P. Comba, G. Rajaraman, H. Rohwer, *Inorg. Chem.* **2007**, *46*, 3826–3838.

